

MicroRNAs Activate Natural Killer Cells through Toll-like Receptor Signaling

Shun He^{1,2}, Jianhong Chu^{1,2}, Lai-Chu Wu³, Hsiaoyin Mao⁴, Yong Peng⁴, Christopher A. Alvarez-Breckenridge¹, Tiffany Hughes⁴, Min Wei⁴, Jianying Zhang⁵, Shunzong Yuan¹, Sumeet Sandhu¹, Sumithira Vasu^{1,2,6}, Don M. Benson Jr.^{1,2}, Craig Hofmeister^{1,2}, Xiaoming He^{1,7}, Kalpana Ghoshal^{1,8}, Steven M. Devine^{1,2,6}, Michael A Caligiuri^{1,2,6,*}, and Jianhua Yu^{1,2,6,*}

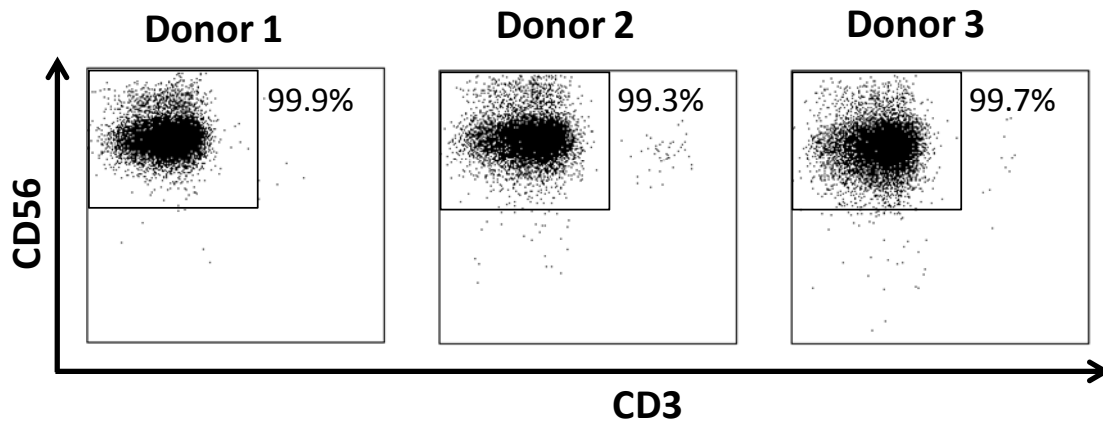
¹The Ohio State University Comprehensive Cancer Center, Columbus, Ohio 43210, USA; ²Division of Hematology, Department of Internal Medicine, College of Medicine, The Ohio State University, Columbus, Ohio 43210, USA; ³Department of Molecular and Cellular Biochemistry, School of Biomedical Science, The Ohio State University, Columbus, OH 43210, USA; ⁴Department of Molecular Virology, Immunology, and Medical Genetics, School of Biomedical Science, The Ohio State University, Columbus, Ohio 43210, USA; ⁵Center for Biostatistics, The Ohio State University, Columbus, Ohio 43210, USA; ⁶Blood and Marrow Transplantation Program, The James Cancer Hospital, The Ohio State University, Columbus, Ohio 43210, USA; ⁷Department of Biomedical Engineering, The Ohio State University, Columbus, Ohio 43210, USA; ⁸Department of Pathology, College of Medicine, The Ohio State University, Columbus, Ohio 43210, USA

Running title: **NK Cell Activation by MicroRNAs**

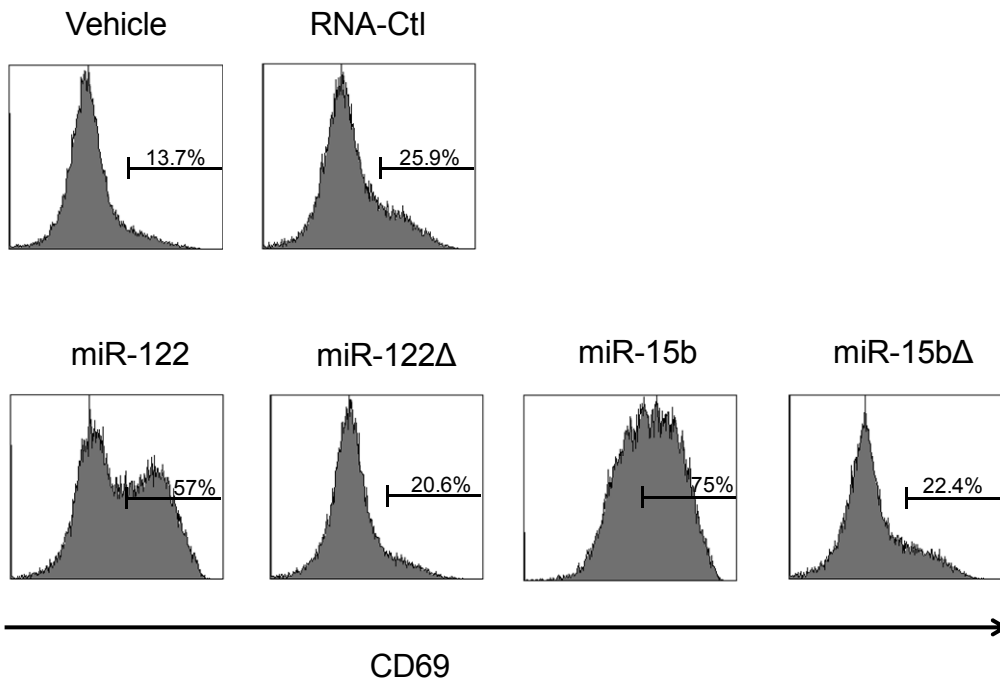
***Correspondence:** Jianhua Yu, Ph.D. or Michael A. Caligiuri, M.D., The Ohio State University, Biomedical Research Tower 816, 460 West 12th Avenue, Columbus, OH 43210. Phone: (614)-292-4158; Fax: (614)-688-4028; Email: Jianhua.yu@osumc.edu or Michael.caligiuri@osumc.edu.

Supplemental Information

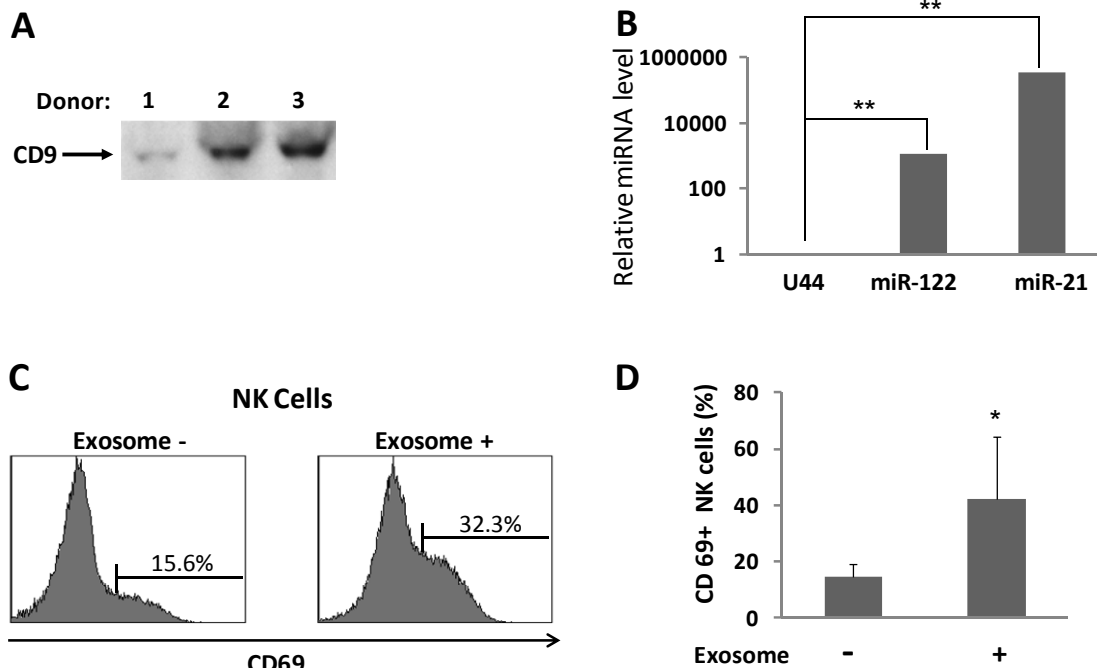
Supplemental Figure S1. Purification of human NK cells. Flow data from 3 representative donors indicate that NK purity is $\geq 99\%$ following negative enrichment with RosetteSep and positive selection with anti-CD56 MACS beads.



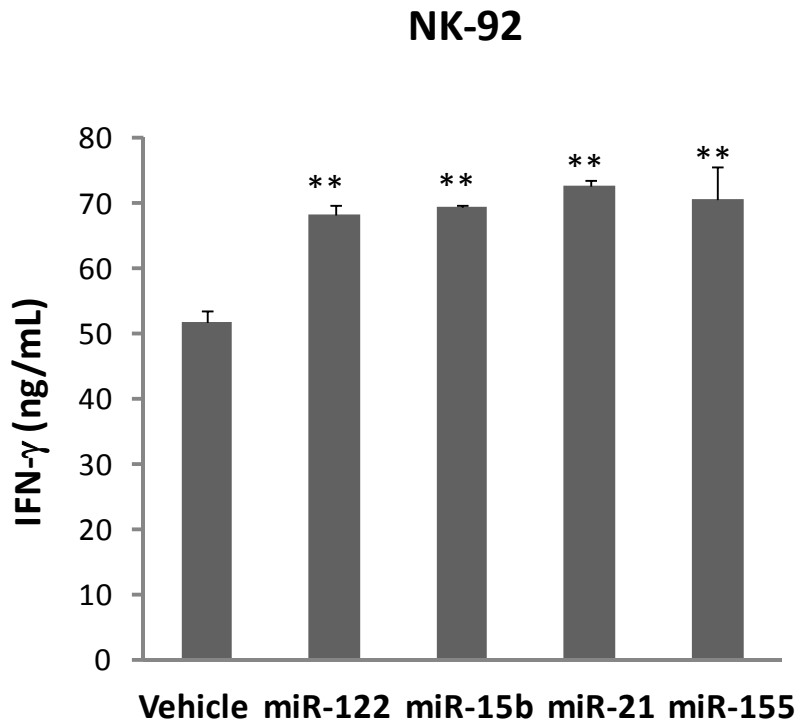
Supplemental Figure S2. Mutation of miRNAs significantly impairs NK cell activation induced by miRNAs. MiR-122 and miR-15b mutants were created by substituting uridines (Us) with guanosine (Gs). Purified human NK cells were stimulated with RNA-Ctl (RNU44), WT miR-122, WT miR-15b, mutated miR-122 (miR-122 Δ), or mutated miR-15b (miR-15b Δ) for 36 hr in the presence of low-dose IL-12. The stimulated NK cells were then harvested, stained and subjected to flow cytometric analysis to detect CD69 expression.



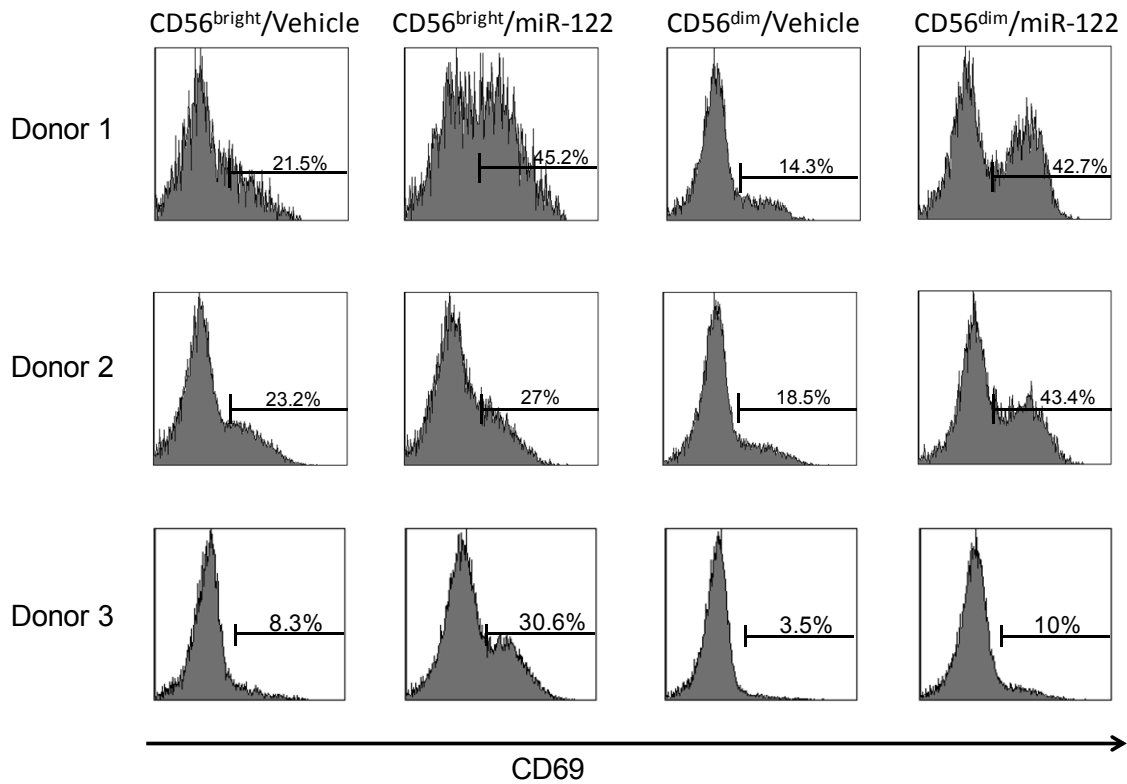
Supplemental Figure S3. MiRNA-containing exosomes induce NK cell activation *ex vivo*. (A) Exosomes were isolated from serum of healthy donors with ExoQuick Exosome (System Biosciences). Exosomes were verified by CD9 expression determined by Western blotting. (B) Purified exosomes were further subjected to RNA extraction, and miR-122 and miR-21 expression levels were detected with Real-time RT-PCR using TaqMan miRNA assays. Small nuclear RNA RNU44 was also included as a control. Results indicate that exosomes contain high levels of miRNAs including miR-122 and miR-21, which were included in this study assessing NK cell activation. (C) Extracted exosomes were added to NK cells purified from the corresponding (autologous) donors and incubated for 36 hr. The NK cells were then harvested and subjected to flow cytometric analysis to detect CD69 surface expression. (D) Summary data of NK cell activation by exosomes for 5 normal human donors. * indicates $P < 0.05$ and ** $P < 0.01$.



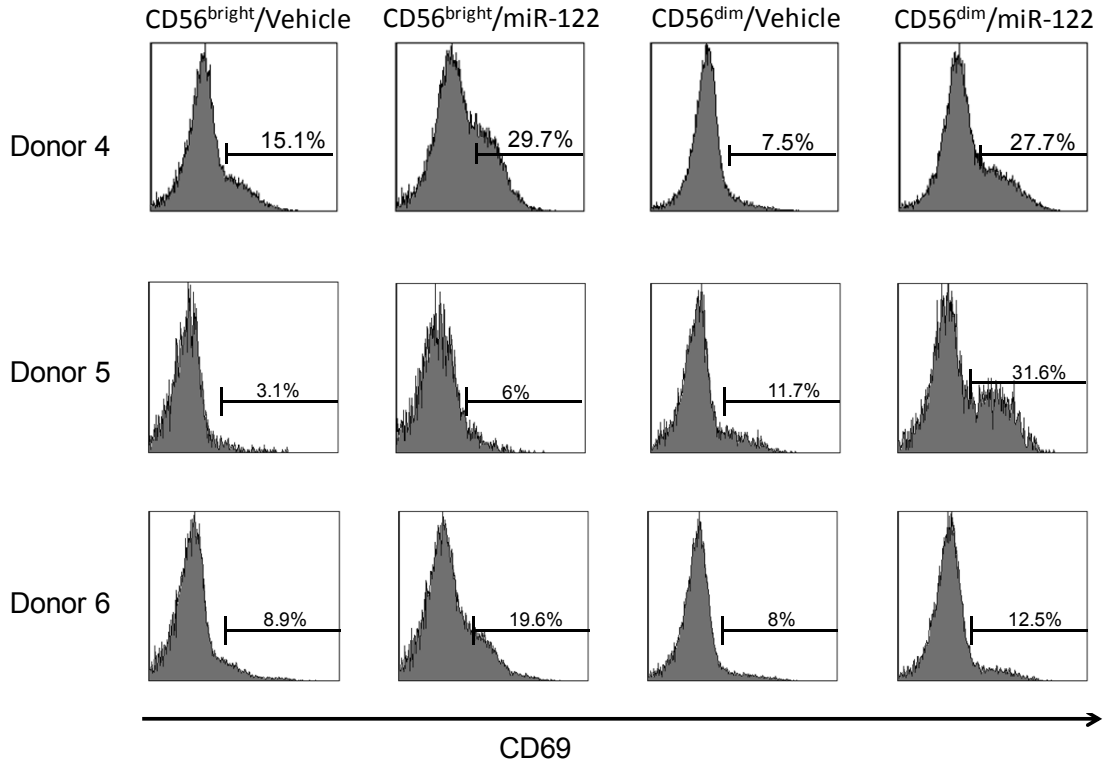
Supplemental Figure S4. MiRNAs enhance IFN- γ production by NK-92 cells. NK-92 cells were starved of IL-2 overnight, and were subsequently treated with miRNAs or DOTAP vehicle control for 36 h in the presence of a low dose of IL-12. Supernatants were harvested to measure IFN- γ production via ELISA. Data shown represent 1 of 3 experiments with similar data. ** indicates $p < 0.01$ and error bars represent S.D.



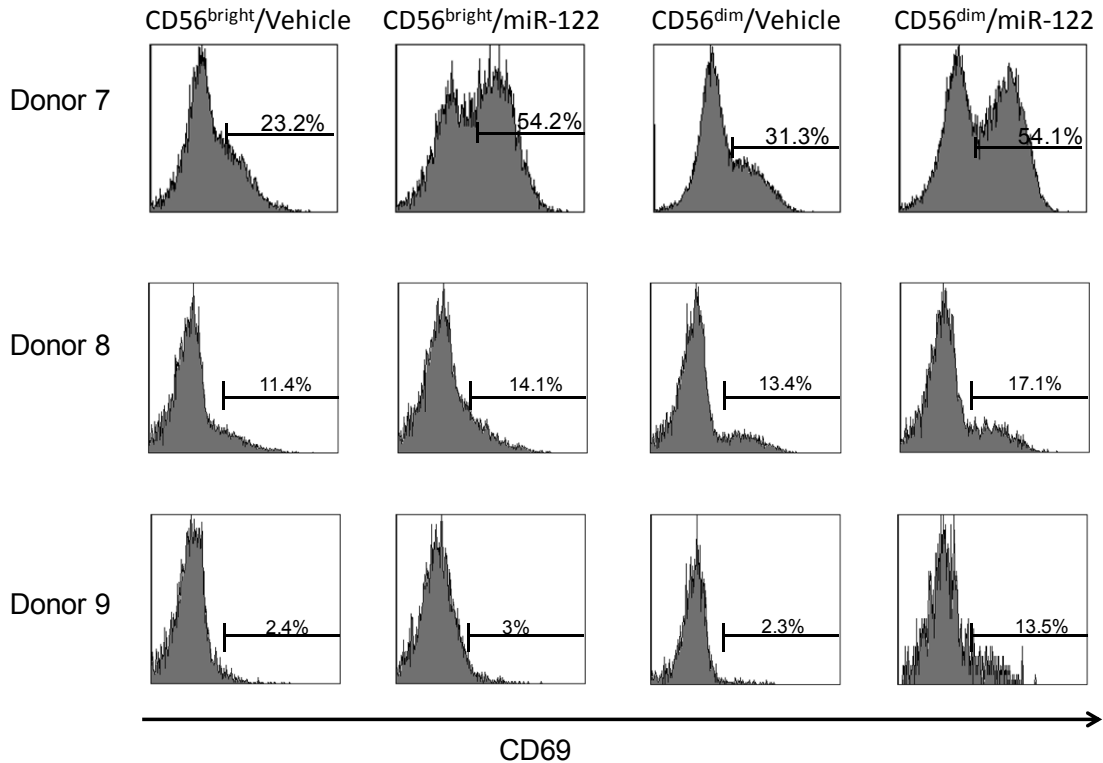
Supplemental Figure S5. MiRNAs induce activation of both CD56^{bright} and CD56^{dim} NK cells. Highly purified human CD56^{bright} and CD56^{dim} NK cells from different donors were sorted. NK cells were gated as CD3⁻CD56⁺. The sorted CD56^{bright} and CD56^{dim} NK cell were then stimulated with vehicle control or miR-122 in the presence of low-dose of IL-12 for 36 hr. The stimulated cells were harvested and subjected to flow cytometric analysis to detect CD69 expression (A). Cell-free supernatants were also collected to determine the levels of IFN- γ secretion via ELISA (B).



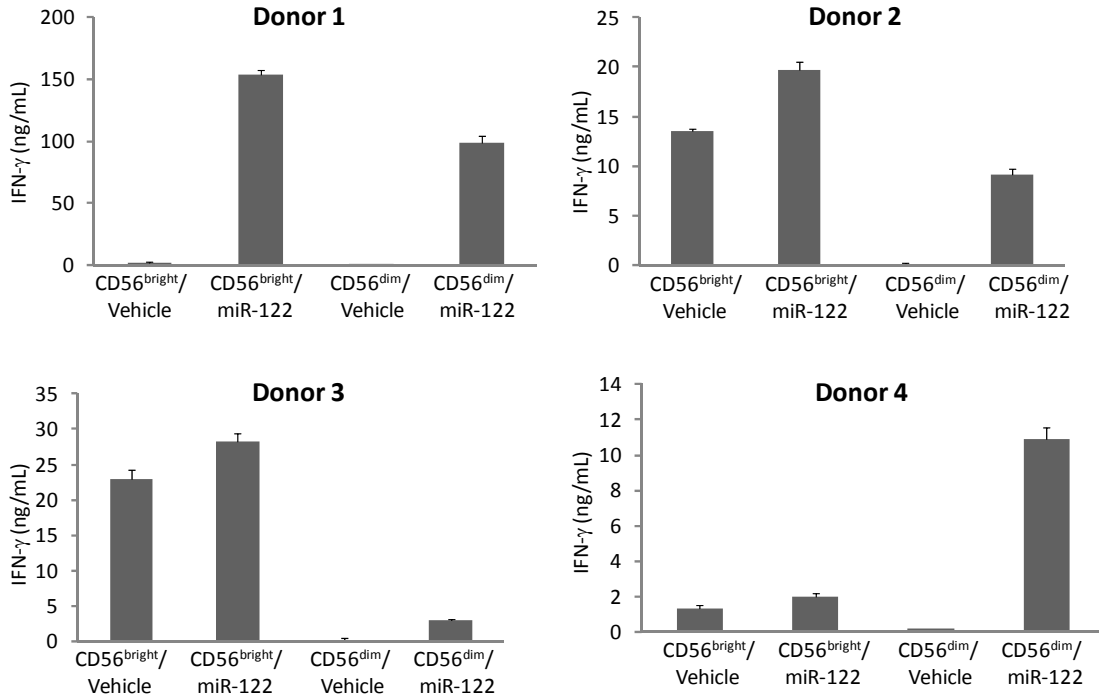
Supplemental Figure S5A continued



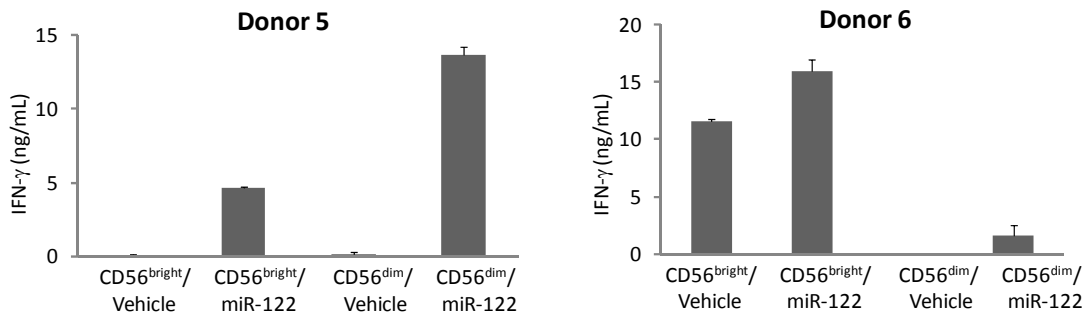
Supplemental Figure 5A continued



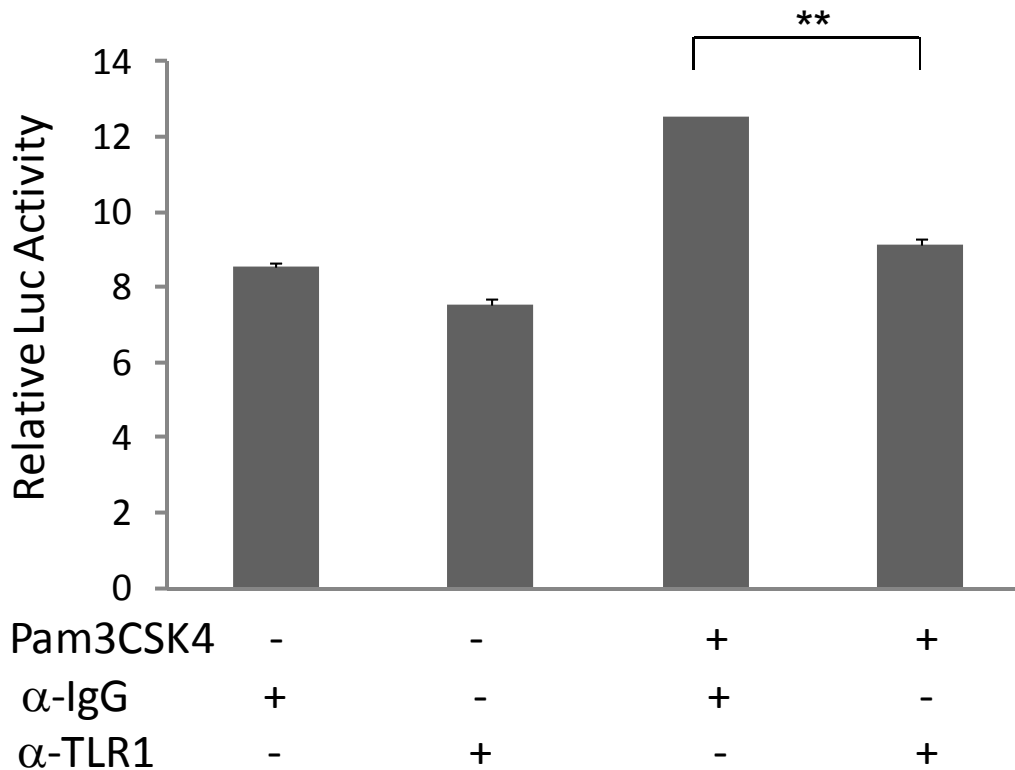
Supplemental Figure S5B



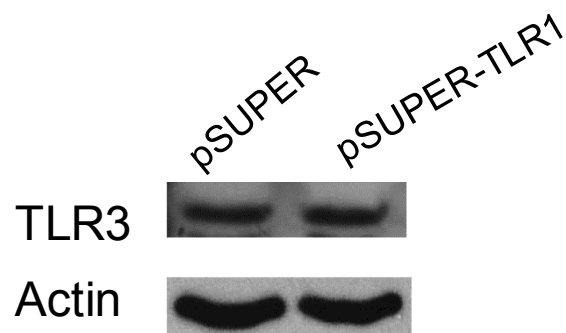
Supplemental Figure S5B continued



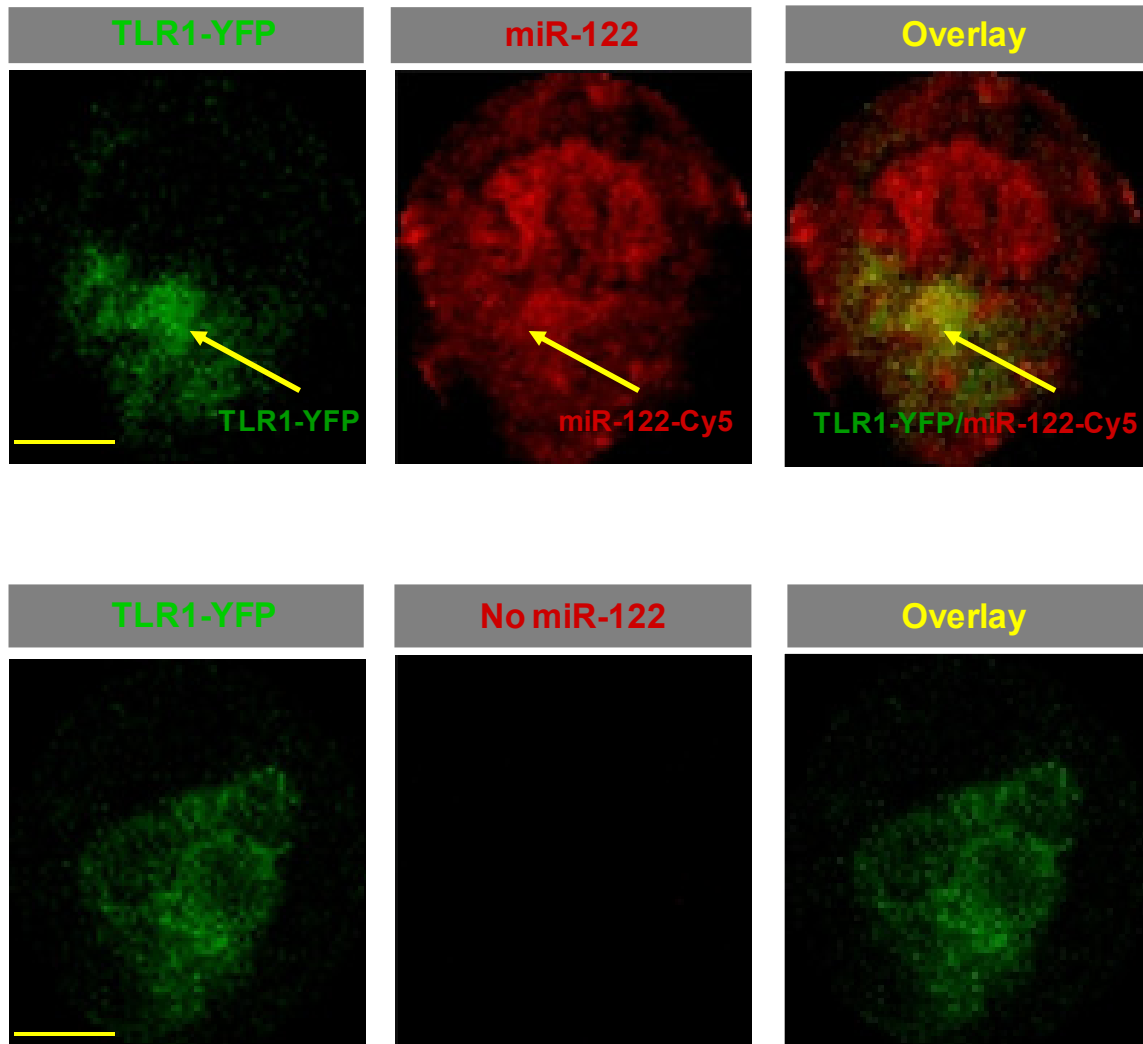
Supplemental Figure S6. Anti-TLR1 antibody effectively blocks the TLR1-NF- κ B signaling activation by Pam3CSK4 ligand. 293T cells were transfected in 24-well plates for 24 hr with TLR1 and TLR2 expression plasmids (0.5 μ g for each) along with pGL-3 κ B-luc (1 μ g), containing three consensus κ B-binding sites, and pRL-TK renilla-luciferase control plasmid (5 ng, Promega). The cells were then incubated with either TLR1 blocking antibody or IgG control (10 μ g/ml for each) for 2 h, followed by treatment with the TLR1 ligand Pam3CSK4 (2 ng/ml) for additional 24 h. Firefly and renilla luciferase activities were measured using Dual-Luciferase® Reporter Assay System (Promega), and the relative activity was determined by the ratio of these two luciferase activities. ** indicates $p < 0.01$ and error bars represent S.D.



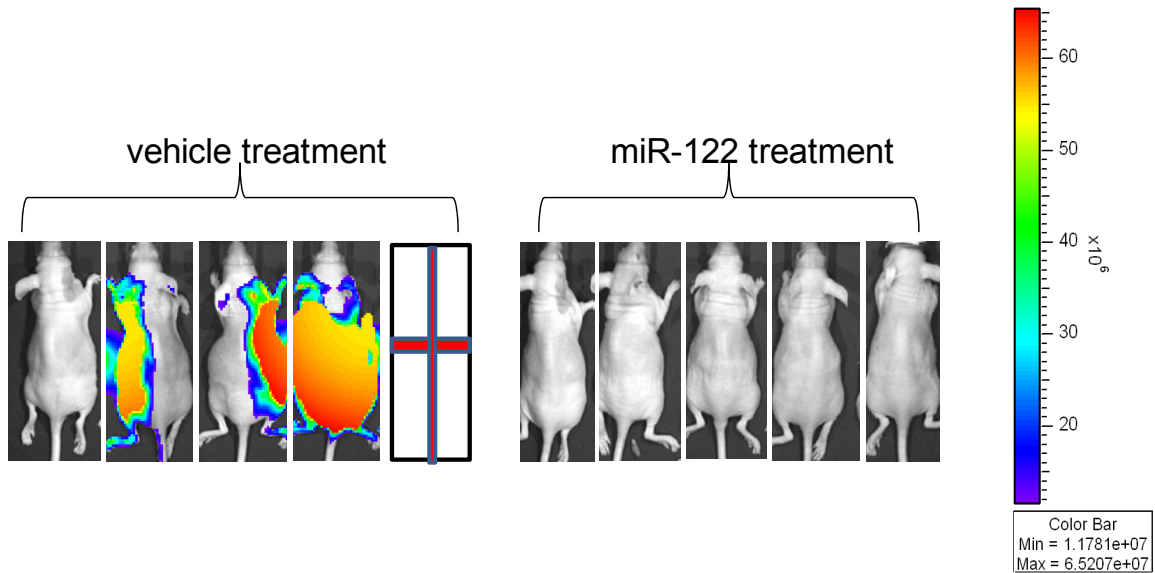
Supplemental Figure S7. TLR1 knockdown cells do not have a decreased TLR3 expression. NK-92 cells were infected with pSUPER-TLR1-GFP or the control retroviruses, and stably transduced cells were sorted based on GFP expression. Both vector-transduced cells (pSUPER) and TLR1 knockdown cells (pSUPER-TLR1) were lysed for Western blotting using a TLR3 antibody (Thermal Scientific Inc.). The same membrane was blotted with β -actin to demonstrate equivalent loading of the samples. Data show that TLR3 is not knocked down by TLR1 shRNA in a pSUPER vector.



Supplemental Figure S8. Co-localization of TLR1 and miRNAs. HEK293T cells were grown on glass cover slips in 6-well plates and transfected with 4 μ g TLR1-YFP plasmids (Addgene). 24 h later, the transfected cells were stimulated with or without 10 μ g/ml Cy5-labeled miR-122 in complexes of DOTAP for 12 h. The coverslips were then washed and mounted on the glass slides using the Prolong Gold Antifade Reagent (Invitrogen). Confocal images were acquired using a Zeiss 510 META laser-scanning confocal microscope. Scale bar (the horizontal and yellow line at the left, bottom corner): 5 μ m.



Supplemental Figure S9. MiRNA treatment significantly suppressed tumor growth in vivo. Ventral bioluminescence imaging of mice bearing A20 lymphoma. Athymic nude mice (5 mice per group) were injected with 1×10^5 luciferase-expressing A20 cells via tail veins and subjected to miRNA or vehicle stimulation three times per week for 4 consecutive weeks. One of the mice in the vehicle group died of tumor before its images were taken and was represented as a red cross.



Supplemental Figure S10. Expression of TLR1 in lymphoma patient NK cells. NK cells were isolated from PBMCs of both healthy donors and lymphoma patients as described in the Materials and Methods. The purified NK cells were then subjected to RNA extraction and cDNA synthesis. The expression level of TLR1 was determined by SYBR Green Real-time PCR assay.

